Nonlinear Dynamics and Control of a Pneumatic Vibration Isolator

Marcel Heertjes
Philips Applied Technologies,
PO Box 218, SAQ-1137,
5600 MD Eindhoven,
The Netherlands
e-mail: marcel.heertjes@philips.com

Nathan van de Wouw
Department of Mechanical Engineering,
Eindhoven University of Technology,
PO Box 513/W-Hoog -1.127,
5600 MB Eindhoven,
The Netherlands
e-mail: N.v.d.Wouw@tue.nl

The nonlinear dynamics of a single-degree-of-freedom pneumatic vibration isolator are studied. Based on a physical model, a nonsymmetric stiffness nonlinearity is derived to describe the stiffness property of the isolator. For a full nonlinear pneumatic isolator model, the response to two different types of disturbances is studied: forces applied to the isolated payload and base vibrations. The dynamic behavior of the isolator in case of a disturbance applied to the payload is studied using the generalized force-mobility function and features coexisting steady-state responses and a superharmonic resonance. Base vibrations transmitted via the isolator are studied on the basis of the generalized transmissibility function again showing rich nonlinear dynamic behavior. The presence of a nonsymmetric nonlinearity also induces high-energy low-frequency response to multiple high-frequency excitation. For both types of excitation, the nonlinear behavior is seriously compromising the performance of the isolator. To avoid any expression of nonlinearity whatsoever and, at the same time, to enhance the performance of the passive isolator, an overall nonlinear control design is proposed. It consists of a linear PID-based controller together with a nonlinear computed torque controller (CTC). For either linear or nonlinear control, the isolator performance is quantified in terms of generalized force mobility and transmissibility. The latter with a special focus on multiple high-frequency excitation. [DOI: 10.1115/1.2128642]

Keywords: active vibration isolation, feedback linearization, generalized force-mobility function, generalized transmissibility function, nonlinear dynamics, pneumatics

1 Introduction

Pneumatic vibration isolators are used to isolate machinery from vibrations [1], e.g., in wafer scanners used to fabricate integrated circuits [2] or in electron microscopes used for submicron imaging. Compared to mechanical or electromechanical devices, pneumatic isolators combine the ability to support large masses with a small stiffness characteristic. Apart from isolating machinery from base vibrations, reducing the sensitivity to vibrations induced by the machinery itself is of major importance. The isolation of machinery from base vibrations is usually characterized by the transmissibility function, i.e., the transfer between base and machine vibrations. Traditionally, the sensitivity to vibrations induced by the machinery itself is characterized by the force-mobility function, i.e., the transfer between machinery-induced forces and the machine's response. Within the framework of linear system theory, both transfer functions provide insight into isolator performance and can be used to express inherent design limitations encountered within the vibration isolation concept [3].

The usage of linear models as a means to describe the behavior of pneumatic vibration isolators is often justified given the range of parameter settings of characteristic system properties, e.g., the isolator effective area for pressure or the payload mass. Outside this range, the nonlinear behavior may quickly prevail over the linear behavior. In [4,5], the nonlinear behavior of vibration isolators is studied. The nonlinear restoring forces are modeled as being symmetric, polynomial (cubic) nonlinearities. In [6], also the effect of nonsymmetric restoring forces is studied, but still these nonlinearities are of a polynomial form. Physical modeling of pneumatic isolators is discussed in [7]. We will show that modeling based on physical reasoning results in a nonsymmetric nonlinearity due to the combined hardening and softening stiffness characteristics inherent to pneumatic isolators. If the isolator volume is decreased under constant pressure, then the resulting stiffness increases, i.e., the system shows hardening behavior on this side of the static equilibrium state. If, however, the isolator volume is increased, then the resulting stiffness decreases and the system shows softening behavior on the opposite side of the static equilibrium state.

For a nonsymmetric nonlinearity, high-frequency disturbance rejection is no longer described by the linear vibration isolation concept. Typically, high-frequency floor vibrations can yield large low-frequency responses of the machine, which is obviously undesirable. As a result, the passive vibration isolation properties are not satisfactory making active vibration isolation a necessary step. In literature, active vibration isolation is often based on linear control techniques (see, for example, [8–10]). In [11], an optimization technique for designing both active and passive nonlinear vibration isolators is proposed. The application of nonlinear control techniques seems rare. In attaining desired performance, we adopt a control strategy combining feedback linearization techniques [12] with a linear loop-shaping controller. The robustness of this partially model-based control design in the face of model parameter uncertainty and measurement noise is studied.

The paper is organized as follows. In Sec. 2, a nonlinear model for a pneumatic isolator is discussed. Its isolation performance with respect to both force excitations (on the machine) and base vibrations is assessed in Sec. 3 in case of harmonic excitations as well as excitations consisting of multiple frequencies. In Sec. 4, the controller design and performance of the active vibration isolator are discussed. Finally, in Sec. 5, conclusions are presented.

2 Pneumatic Vibration Isolator Model

Pneumatic vibration isolators are generally modeled using standard mechanical components, such as masses, springs, and dampers. In this regard, the simplified mass-spring-damper model, such as depicted in Fig. 1 via conventional and block-form representation, is often considered. It consists of a payload mass m, a damper describing the linear relation between input velocity and output force via the constant b, and a spring describing the linear

Contributed by the Technical Committee on Vibration and Sound of ASME for publication in the Journal of Vibration and Acoustics. Manuscript received October 13, 2003; final manuscript received April 11, 2005. Assoc. Editor: Joseph P. Cusumano.

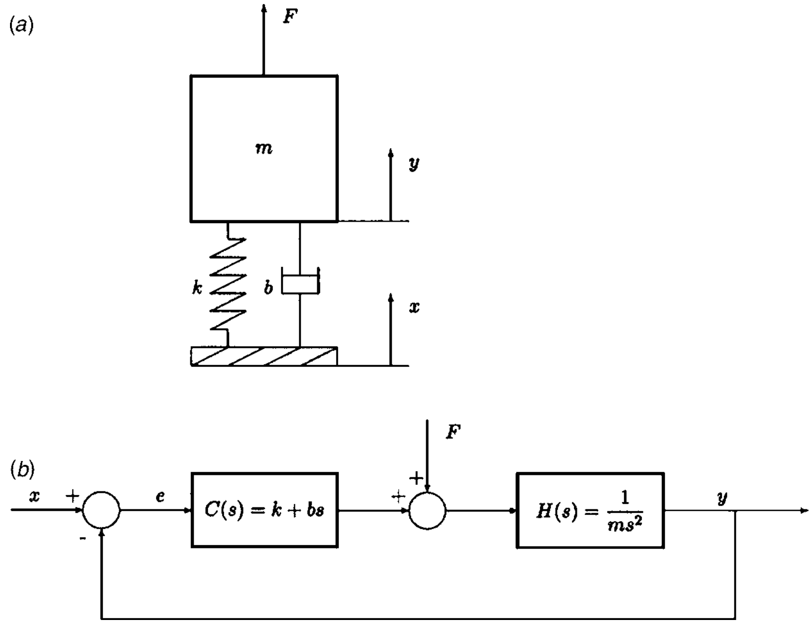

Fig. 1 Conventional (*a*) and block-form (*b*) representation (in the Laplace domain) of a vibration isolator model under base and force excitation

relation between input displacement and output force via the constant k. The model is subjected to a base disturbance x and a force disturbance F. In this way, we discriminate between disturbances acting indirectly on the payload mass, e.g., floor vibrations, and disturbances acting directly on the payload mass, e.g., parasitic dynamics and pneumatic or acoustic noise. The absolute displacement of the payload mass is given by y, which often represents the variable to be controlled.

The objective in vibration isolation is to isolate the payload mass m from both base and force disturbances. To quantify the ability of the isolator to do so, two performance measures are considered: the so-called transmissibility function, or

$$T(s) = \frac{Y(s)}{X(s)} = \frac{bs + k}{ms^2 + bs + k} \tag{1}$$

and, traditionally, the force-mobility function,

$$T_f(s) = \frac{sY(s)}{F(s)} = \frac{s}{ms^2 + bs + k} \tag{2}$$

where $Y(s)=\mathcal{L}(y(t))$, $X(s)=\mathcal{L}(x(t))$, and $F(s)=\mathcal{L}(F(t))$ are the Laplace transforms of $y(t)$, $x(t)$, and $F(t)$, respectively. Both transfer functions can be used to illustrate fundamental trade-offs in the linear vibration isolation concept. For example, to isolate the payload mass from high-frequency base motion, the natural frequency $\omega_n = \sqrt{k/m}$ should be chosen as small as possible. Given a payload mass m, this implies that k should be chosen as small as possible. In terms of force mobility, however, k should be chosen as large as possible as to improve low-frequency disturbance rejection. This represents a trade-off, which, mathematically, is illustrated by

$$T(s) + \frac{T_f(s)}{sH(s)} = 1 \tag{3}$$

i.e., given $H(s)$ performance improvement in $T(s)$ may imply performance deterioration in $T_f(s)$ or vice versa. The vibration isolation concept offers the possibility of choosing passive or active vibration isolator properties in a straightforward and comprehensive way given the fundamental performance limitations.

To study the consequences of nonlinear isolator dynamics within this concept, a nonlinear relation between input displacement and output force is derived on the basis of Poisson's law for adiabatic processes, or

$$pV^\kappa = P_o V_o^\kappa, \quad \kappa = \frac{c_p}{c_V} \approx 1.402 \tag{4}$$

with p the isolator pressure, V the isolator volume, P_o the static isolator pressure, and V_o its corresponding volume. The constants P_o and V_o are given by

$$P_o = p_o + \frac{mg}{A_p} \quad \text{and} \quad V_o = L_o A_v \tag{5}$$

where p_o represents the atmospheric pressure, g the gravitational acceleration, A_p the effective area for pressure, L_o the static chamber length, and A_v the effective area for volume. The ratio between the constant pressure specific heat c_p and the constant volume specific heat c_V is represented by κ. From Eq. (4), it follows that a nonlinear relation between isolator pressure p and isolator length $L(x,y)$ is given by

$$p = \left(p_o + \frac{mg}{A_p}\right)\left(\frac{L_o}{L(x,y)}\right)^\kappa \tag{6}$$

with $L(x,y)=L_o+y-x$. Differentiation of Eq. (4) with respect to V yields

$$\frac{dp}{dV} = -\kappa\frac{p}{V} \tag{7}$$

which after substitution of Eq. (6), $dpA_p=-dF$, and $dV=A_V dL$, gives the following nonlinear stiffness characteristic of the isolator:

$$\frac{dF}{dL} = \kappa(x,y) = \frac{\kappa(A_p p_o + mg)}{L_o}\left(\frac{L_o}{L(x,y)}\right)^{\kappa+1} \tag{8}$$

It follows that $k(x,y)$ depends on the volume, i.e., it only represents a constant if the volume is assumed to be constant, in which case it is determined by the static equilibrium state, i.e.,

$$k = \frac{\kappa(A_p p_o + mg)}{L_o} \quad (9)$$

This volume dependency forms the basis of a nonlinear restoring force: increasing the volume decreases $k(x,y)$, whereas decreasing the volume increases $k(x,y)$, see also [13].

3 Nonlinear Isolator Performance Assessment

To assess the nonlinear isolator performance within the vibration isolation concept, performance of the passive pneumatic isolator in the presence of force excitation (Sec. 3.1) and base vibrations (Sec. 3.2) is studied. Under harmonic-force excitation, characteristic nonlinear dynamic behavior will be discussed. In addition—under base vibrations—also high-frequency excitation with multiple frequency components will be considered. Such vibrations are assumed to be realizations of stochastic processes containing energy in a high-frequency band.

3.1 Force Excitation. For the considered pneumatic vibration isolator that is merely subjected to harmonic-force excitation, see Fig. 1 with $x=0$ and the nonlinear restoring characteristic as discussed in Sec. 2, the following equation of motion can be derived:

$$m\frac{d^2y}{dt^2} + b\frac{dy}{dt} + k(y)y = \hat{F}\cos(2\pi ft) \quad (10)$$

with $\hat{F}$ the amplitude of harmonic excitation and f the excitation frequency. The nonlinear stiffness function $k(y)$, defined by Eq. (8), can be written as

$$k(y) = k\left(1 - \frac{y}{y+L_o}\right)^{\kappa+1} \quad (11)$$

By itself $k(y)$ consists of a constant and a state-dependent part clearly representing a nonsymmetric nonlinearity. By introducing the following set of dimensionless variables ξ and θ for displacement and time, respectively, and the dimensionless parameter ζ for damping according to

$$\xi = \frac{k}{\hat{F}}y, \quad \theta = \sqrt{\frac{k}{m}}t, \quad \text{and} \quad \zeta = \frac{b}{2\sqrt{mk}} \quad (12)$$

the equation of motion Eq. (10) can be written in the dimensionless form,

$$\frac{d^2\xi}{d\theta^2} + 2\zeta\frac{d\xi}{d\theta} + \mathcal{K}(\xi)\xi = \cos(\Omega\theta) \quad (13)$$

with

$$\mathcal{K}(\xi) = \left(\frac{\phi}{\xi+\phi}\right)^{\kappa+1}, \quad \phi = \frac{L_o k}{\hat{F}}, \quad \text{and } \Omega = 2\pi f\sqrt{\frac{m}{k}} \quad (14)$$

From Eqs. (13) and (14), it can be concluded that the degree of nonlinearity strongly depends on the parameter ϕ. It does not seem to depend on the static chamber length L_o because with Eq. (9) ϕ can be written as

$$\phi = \frac{L_o k}{\hat{F}} = \frac{\kappa(A_p p_o + mg)}{\hat{F}} \quad (15)$$

Via numerical simulation with Eq. (13), the vibration isolation performance in case of harmonic-force excitation is quantified; force excitation typically concerns pneumatic disturbances, such as dither applied to valves, acoustic excitation resulting from air conditioning systems, but also the vibrational influence of additional dynamics acting on the payload mass. So-called period-1 solutions for which the period time equals the period time of excitation are computed for different values of the dimensionless excitation frequency Ω using a combination of a finite-difference method and a path-following technique [14]. The graphical representation of these solutions is given by the generalized force-mobility function. Different from its linear equivalent, see Eq. (2), the generalized force-mobility function is obtained by computing the maximum absolute value of the periodic velocity of the payload mass—in dimensionless form $d\xi_{p-1}/d\theta$—after subjecting the system to a harmonic (period-1) force excitation at specific values of Ω. It expresses the sensitivity of the vibration isolator to disturbances acting on the system itself, whereas, in the absence of nonlinearity, it equals the amplitude characteristic of the force-mobility function. For the considered pneumatic vibration isolator, the generalized force-mobility function is depicted in Fig. 2.

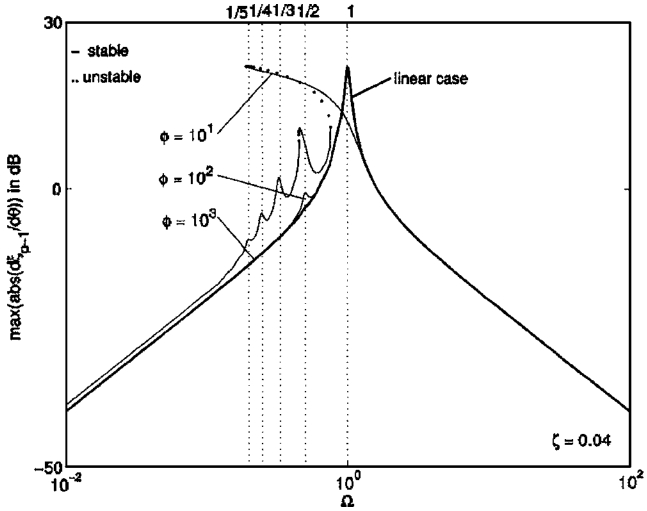

Fig. 2 Generalized force-mobility function (amplitude characteristic)

For the linear case, it can be seen that the generalized force-mobility function has its peak value at resonance, i.e., $\Omega=1$. This peak value can be influenced by the damping coefficient ζ. For high values of ϕ, i.e., $\phi=10^3$ corresponding to a small degree of nonlinearity, the generalized force-mobility function resembles the linear force-mobility function. For $\phi=10^2$, an additional resonance appears near half the linear resonance frequency, $\Omega=1/2$, hence, a second superharmonic resonance. For $\phi=10$, excessive nonlinear dynamic behavior is found in the form of multiple superharmonic resonances, a low-frequency offset value, and a resonance peak bending to the left. The latter results in a frequency region where multiple (stable and unstable) periodic solutions coexist. It demonstrates that vibration isolation in the presence of nonlinearity can be seriously compromised in the frequency range just below the linear resonance frequency.

3.2 Base Excitation. For the pneumatic vibration isolator that is subjected to harmonic base excitation (see Fig. 1 with $F=0$ combined with the nonlinear restoring characteristic as discussed in Sec. 2), the following equation of motion can be derived:

$$m\frac{d^2y}{dt^2} + b\frac{dy}{dt} + k(x,y)y = b\frac{dx}{dt} + k(x,y)x, \quad x = \hat{x}\cos(2\pi ft) \quad (16)$$

with $\hat{x}$ the amplitude of harmonic excitation and f the excitation frequency. The nonlinear force characteristic $k(x,y)$ follows from Eq. (8), or

$$k(x,y) = k\left(1 - \frac{(y-x)}{(y-x)+L_o}\right)^{\kappa+1} \quad (17)$$

and, similar to the case of force excitation, represents a nonsymmetric stiffness nonlinearity. By introducing the following dimensionless variables:

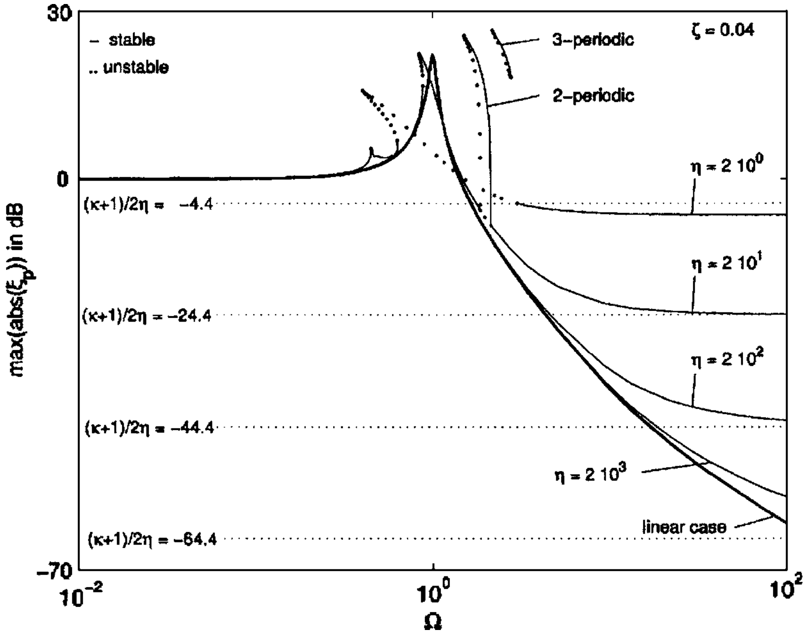

Fig. 3 Generalized transmissibility function (amplitude characteristic)

$$\xi = \frac{y}{\hat{x}}, \quad \theta = \sqrt{\frac{k}{m}}t, \quad \text{and } \zeta = \frac{b}{2\sqrt{mk}} \tag{18}$$

this equation of motion can be written in the dimensionless form,

$$\frac{d^2\xi}{d\theta^2} + 2\zeta\frac{d\xi}{d\theta} + \mathcal{K}(\xi,\theta)\xi = -2\zeta\Omega\sin(\Omega\theta) + \mathcal{K}(\xi,\theta)\cos(\Omega\theta) \tag{19}$$

with

$$\mathcal{K}(\xi,\theta) = \left(\frac{\eta}{\eta + \xi - \cos(\Omega\theta)}\right)^{\kappa+1}, \quad \eta = \frac{L_o}{\hat{x}}, \quad \text{and } \Omega = 2\pi f\sqrt{\frac{m}{k}} \tag{20}$$

Two major conclusions can be drawn: (i) the degree of nonlinearity (related to $\mathcal{K}(\xi,\theta)$) strongly depends on the parameter η (i.e., the static equilibrium chamber length L_o and the level of disturbance $\hat{x}$) and (ii) the degree of nonlinearity increases for larger values of ξ typically occurring near resonance (see also [6]).

Using the same numerical tools as were used in Sec. 3.1, periodic solutions of Eq. (19) are computed. The graphical representation of such solutions in a frequency range of interest is provided by the generalized transmissibility function. Different from its linear equivalent, see Eq. (1), the generalized transmissibility function is obtained by depicting the maximum absolute values of the computed periodic solutions—in dimensionless form represented by $\max(\text{abs}(\xi_p))$—within a frequency range of interest. For this frequency range, it expresses isolation performance and equals the amplitude characteristic of the linear transmissibility frequency response function in the absence of nonlinearity. For the considered pneumatic vibration isolator, the generalized transmissibility function is depicted in Fig. 3 at various values of η.

For the low-frequency range, i.e., below $\Omega = 1$, it can be seen that the maximum absolute value of the period-1 response equals the amplitude of the base excitation; hence, no vibration isolation is obtained. For the high-frequency range, i.e., beyond $\Omega = 1$, the maximum absolute value of the period-1 response will become smaller than the amplitude of base excitation, i.e., vibration isolation is obtained. The amount of amplification of base vibrations near resonance depends on the amount of damping ζ. Clearly for large values of η, corresponding to a small degree of nonlinearity, the nonlinear transmissibility function resembles its linear equivalent. For smaller values of η, corresponding to a larger degree of nonlinearity, distinct nonlinear effects appear: bending of the resonance peak, multiple coexisting solutions, and both period-2 and period-3 behavior. Figure 3 also shows an offset value present in the nonlinear system response; see the horizontal dashed lines. By itself, such an offset value should not compromise isolation performance. However, it results from the nonsymmetric stiffness characteristic, which also has the potential of having high-frequency excitations (consisting of multiple frequency components) induce large low-frequency responses, the type of excitations for which the isolator is designed to deliver a high level of disturbance attenuation.

To study the nonsymmetric stiffness characteristic, or, more specifically, its effect on the system response, a Taylor series expansion of the nonlinearity is employed via a second-order approximation of the nonlinear terms in Eq. (19)

$$\begin{aligned}\mathcal{K}(\xi,\theta)[\xi - \cos(\Omega\theta)] &= \left(\frac{\eta}{\eta + \xi - \cos(\Omega\theta)}\right)^{\kappa+1}[\xi - \cos(\Omega\theta)] \\ &\approx \xi - \cos(\Omega\theta) - \frac{\kappa+1}{\eta}[\xi - \cos(\Omega\theta)]^2\end{aligned} \tag{21}$$

With this approximation, Eq. (19) is written as

$$\begin{aligned}\frac{d^2\xi}{d\theta^2} + 2\zeta\frac{d\xi}{d\theta} + \xi - \frac{\kappa+1}{\eta}\xi^2 &= -2\zeta\Omega\sin(\Omega\theta) + \frac{\kappa+1}{\eta}\cos^2(\Omega\theta) \\ &+ \left(1 - \frac{2(\kappa+1)\xi}{\eta}\right)\cos(\Omega\theta)\end{aligned} \tag{22}$$

which for $\eta > 1$ and $|\xi| \ll 1$ can be further approximated by

$$\frac{d^2\xi}{d\theta^2} + 2\zeta\frac{d\xi}{d\theta} + \xi = -2\zeta\Omega\sin(\Omega\theta) + \cos(\Omega\theta) + \frac{\kappa+1}{\eta}\cos^2(\Omega\theta) \tag{23}$$

The steady-state solution of the resulting linear differential equation is given by

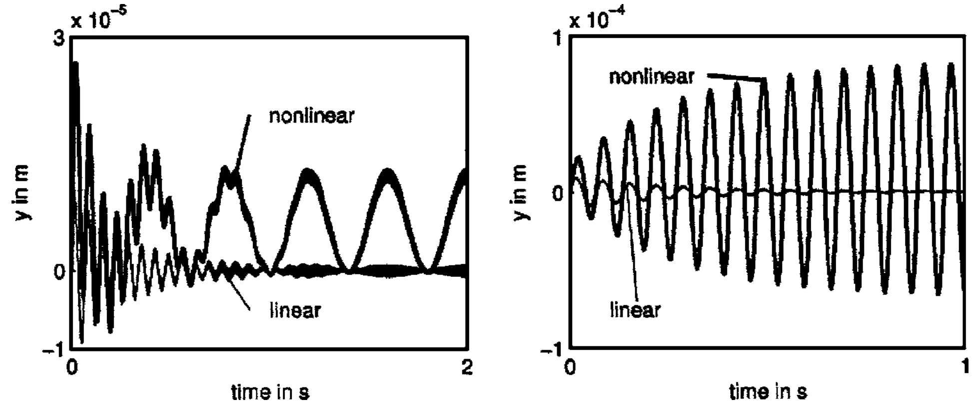

Fig. 4 Response of the linear and nonlinear isolator model under multiple frequency base excitation: $\hat{x}=10^{-4}$ m, $f_1=200$ Hz, $f_2=202.5$ Hz (in the left part), and $f_2=214.75$ Hz (in the right part)

$$\begin{aligned}\xi(\theta) = {} & \frac{\kappa+1}{2\eta} + \frac{(1-\Omega^2)+(2\Omega\zeta)^2}{(1-\Omega^2)^2+(2\Omega\zeta)^2}\cos(\Omega\theta) \\ & + \frac{2\Omega^3\zeta}{(1-\Omega^2)^2+(2\Omega\zeta)^2}\sin(\Omega\theta) \\ & + \frac{(\kappa+1)(1-4\Omega^2)}{2\eta[(1-4\Omega^2)^2+(4\zeta\Omega)^2]}\cos(2\Omega\theta) \\ & + \frac{4(\kappa+1)\zeta\Omega}{2\eta[(1-4\Omega^2)^2+(4\zeta\Omega)^2]}\sin(2\Omega\theta)\end{aligned} \tag{24}$$

Two characteristics appear: (i) an offset value, and (ii) an additional resonance at $\Omega=1/2$. Both features are present (even within a certain degree of accuracy) in the computations with the full nonlinear model, such as shown in Fig. 3.

At this point in the analysis of the nonlinear vibration isolator we will shift our focus from harmonic to nonharmonic vibrations, for example, floor vibrations that exhibit energy in a certain (high-)frequency range [15]. As mentioned before under nonharmonic vibration, the nonsymmetric nature of the nonlinearity can cause severe changes in performance. Often the response of a system with a nonsymmetric nonlinearity exposed to a multiple frequency excitation (ultimately stochastic excitation) will not only contain the individual frequency components of the excitation signal—possibly with higher harmonics—but also contains energy at frequency components that are defined by the difference between the frequency components of excitation (see, for example, [16,17]. As a consequence, low-frequency contributions can result from a purely high-frequency excitation, which—via resonance—can induce a significant deterioration in system performance. For purposes of illustration, time-series computations are performed with the nonlinear isolator model, see Eq. (16), and a dual frequency excitation, i.e.,

$$x = \hat{x}_1\cos(2\pi f_1 t) + \hat{x}_2\cos(2\pi f_2 t) \tag{25}$$

In Eq. (25), $\hat{x}_1=\hat{x}_2=\sqrt{1/2}\hat{x}$ to ensure a comparable excitation level with the previous case of harmonic excitation. Furthermore, $\hat{x}=1.0\times10^{-4}$ m and $L_o=2.0\times10^{-3}$ m, which corresponds to a situation with $\eta=20$. For the case that $f_1=200$ Hz and $f_2=202.5$ Hz, the simulation results for both the nonlinear model as well as the linear model ($k(x,y)=k$ in Eq. (16)) are depicted in the left part of Fig. 4.

This figure clearly illustrates the low-frequency high-amplitude nonlinear response; the difference between the maximum and minimum value of the response is $\approx1.3\times10^{-5}$ m in the nonlinear case as opposed to $\approx1.6\times10^{-6}$ m in the linear case. The response is dominated by the difference in frequency components $f_2-f_1=2.5$ Hz. Obviously, this difference in frequency is not present in the applied excitation signal, see Eq. (25), nor in the linear response. Moreover, the nonlinear response shows an offset value, whereas the linear response does not. For the case that $f_1=200$ Hz and $f_2=214.75$ Hz, the simulation results are depicted in the right part of Fig. 4. The excitation frequencies are chosen such that the difference in frequency components is close to the resonance frequency of the isolator. This yields a difference in maximum and minimum value of the response equal to $\approx1.5\times10^{-4}$ m in the nonlinear case as opposed to 1.8×10^{-6} m in the linear case, hence a performance deterioration by a factor of eighty which is completely due to the presence of nonlinearity. For high-frequency broadband excitation, it is likely that there exist differences in frequency contributions that are close to the resonance frequency, and, thereby, have the potential of inducing a large low-frequency response. Consequently, disturbance attenuation in view of nonlinear pneumatic isolator dynamics may seriously be compromised and passive isolation, in general, may not suffice. This offers a sufficient basis for the application of active control to improve performance.

4 Active Vibration Isolation

Active vibration isolation often refers to a combination of an active and a passive vibration isolation design. Given the considered nonsymmetric passive isolator characteristic, a PID controller (Sec. 4.1) with a second-order low-pass filter is used to shape the isolation properties. In addition to the linear control design, a nonlinear computed torque part (Sec. 4.2) is added as to compensate for nonlinearity in the system. Either for harmonic force excitation or harmonic base excitation, the controlled isolator design is studied with respect to isolation performance in terms of generalized force mobility or generalized transmissibility. In the case of base excitation also high-frequency excitation with multiple frequency components is considered.

4.1 Linear Vibration Control. Often the goal in vibration control is to reduce the sensitivity of the controlled variable to disturbances acting upon the underlying process. Strictly speaking, this poses a problem: the controlled variable cannot be measured because it is represented by the absolute displacement of the payload (see also Sec. 2). In practice, this problem is dealt with by considering two alternatives: (i) measure time derivatives (e.g., absolute velocity or absolute acceleration) or (ii) measure relative displacement. Based on linear control, a combined active-passive vibration isolation design is presented for the second alternative.

In Fig. 5, a control design is shown via block-diagram representation. Here C_a represents a PID controller with an additional second-order low-pass filter, which is given in frequency domain by the transfer function

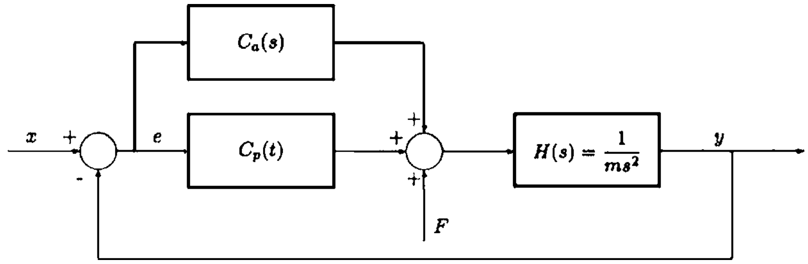

Fig. 5 Block-from representation of a combined passive-active vibration isolation design under base and force excitation

$$C_a(s) = \frac{k^a \omega_{lp}^2 (s^2 + (\omega_d + \omega_i)s + \omega_d \omega_i)}{\omega_d (s^2 + 2\beta \omega_{lp} s^2 + \omega_{lp}^2 s)} \tag{26}$$

with k^a the controller gain, ω_i the break point of the lag filter, ω_d the break point of the lead filter, ω_{lp} the break point of the low-pass filter, and β the corresponding damping coefficient. The choice for this controller structure together with its parameter values reflects the general idea in vibration isolation practice: active control is used as an additive means to shape isolation properties. The isolation function itself is primarily obtained via passive construction elements. To this extent, the lag filter accounts for additional low-frequency disturbance rejection, the lead filter induces active damping near resonance, and the low-pass filter assures controller roll-off in the (high-)frequency range. In Fig. 5, the nonlinear isolator characteristic C_p is given in time domain by

$$C_p(t) = b\frac{dx}{dt} - b\frac{dy}{dt} + k(x,y)x - k(x,y)y \tag{27}$$

with b and k the damping and stiffness coefficient, respectively, and with the nonlinear nonsymmetric stiffness characteristic

$$k(x,y) = k\left(1 - \frac{y-x}{y-x+L_o}\right)^{\kappa+1} \tag{28}$$

where L_o represents the isolator static chamber length, κ the ratio between constant pressure- and volume-specific heat, x the reference displacement, and y the displacement of the payload mass (see also Sec. 2). The payload is represented in frequency domain by the transfer function of a double integrator

$$H(s) = \frac{1}{ms^2} \tag{29}$$

with coefficient m representing the payload mass. The performance of the combined active-passive isolator design is studied under disturbances F or x, i.e., the case of force excitation ($x=0$) and the case of base excitation ($F=0$).

4.1.1 Force Excitation. For the linear controlled nonlinear pneumatic vibration isolator model that is subjected to harmonic force excitation $F=\hat{F}\cos(2\pi f t)$ with excitation amplitude $\hat{F}$ and excitation frequency f (see Fig. 5 with $x=0$), the following dimensionless equations of motion can be derived in matrix notation:

$$\frac{d\Xi}{d\theta} = A(\Xi)\Xi + Bu, \quad u = \cos(\Omega\theta) \tag{30}$$

with

$$A(\Xi) = \begin{bmatrix} 0 & 1 & 0 & 0 & 0 \\ 0 & 0 & 1 & 0 & 0 \\ 0 & -\Omega_{lp}^2 & -2\beta\Omega_{lp} & \Omega_{lp}^2 & 0 \\ 0 & 0 & 0 & 0 & 1 \\ -\alpha\frac{\omega_i}{\omega_n} & -\alpha\left(1 + \frac{\omega_i}{\omega_d}\right) & -\alpha\frac{\omega_n}{\omega_d} & -\mathcal{K}(\Xi_4) & -2\zeta \end{bmatrix}$$

$$\text{and } B = \begin{bmatrix} 0 \\ 0 \\ 0 \\ 0 \\ 1 \end{bmatrix}$$

The vector $\Xi=[\Xi_1\ \Xi_2\ \Xi_3\ \Xi_4\ \Xi_5]^{\mathrm{T}}$ contains the dimensionless displacement and velocity of the payload: $\Xi_4=\xi$ and $\Xi_5=d\xi/d\theta$, respectively. The dimensionless variables: ξ and θ for payload displacement and time, respectively, Ω representing the dimensionless excitation frequency, and ζ representing the dimensionless damping coefficient, are given by

$$\xi = \frac{k}{\hat{F}}y, \quad 0 = \sqrt{\frac{k}{m}}t, \quad \Omega = 2\pi f\sqrt{\frac{m}{k}}, \quad \text{and } \zeta = \frac{b}{2\sqrt{mk}} \tag{31}$$

Furthermore, the dimensionless parameters and/or variables in $A(\Xi)$ are defined as

$$\alpha = \frac{k^a}{k}, \quad \Omega_{lp} = \frac{\omega_{lp}}{\omega_n}, \quad \text{and } \mathcal{K}(\Xi_4) = \left(\frac{\phi}{\Xi_4 + \phi}\right)^{\kappa+1} \tag{32}$$

with $\omega_n=\sqrt{k/m}$ and $\phi=L_o k/\hat{F}$. Note that the degree of nonlinearity in $\mathcal{K}(\Xi_4)$ is largely determined by ϕ, i.e., the characteristic isolator length L_o, the stiffness coefficient k, and the amplitude of force excitation $\hat{F}$. For purposes of numerical analysis, the parameter values in $A(\Xi)$ are given by $\omega_i=\omega_d=\omega_n/5$, $\omega_{lp}=5\omega_n$, $\alpha=1/10$, $\zeta=0.04$, $\kappa\approx 1.402$, and $\beta=1$. Similar values are found in the photolithographic industry for active vibration isolation of metrology frames.

With Eq. (30) a numerical analysis is performed of which the results are shown in Fig. 6 in generalized force-mobility representation. Four curves are depicted of period-1 solutions computed for varying dimensionless excitation frequency Ω. The degree of nonlinearity is expressed by ϕ. Additionally, the passive linear isolator characteristic is depicted. The advantage in system performance by applying additional linear vibration control is shown by comparing the passive linear isolator characteristic with the curve based on $\phi=10^3$. This curve corresponds to an active, almost linear, isolator characteristic. It can be seen that: (i) the lead filter, i.e., the differentiator part in Eq. (26), induces additional disturbance suppression near resonance, (ii) the lag filter, i.e., the integrator part in Eq. (26), induces additional low-frequency distur-

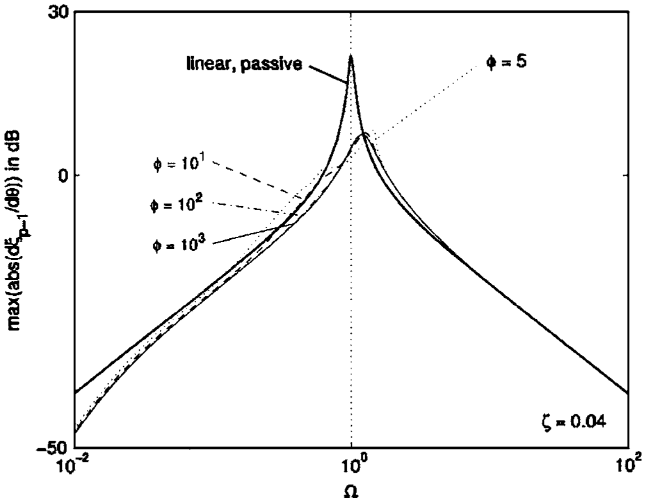

Fig. 6 Generalized force-mobility function (amplitude characteristic)

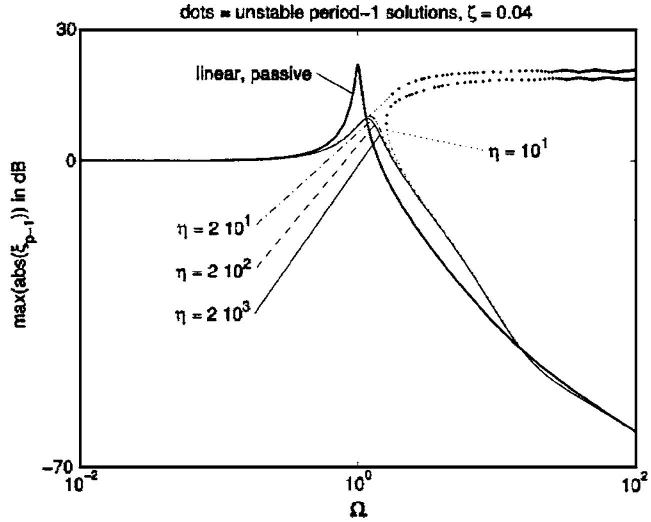

Fig. 7 Generalized transmissibility function (amplitude characteristic)

bance rejection, and (iii) the low-pass filter guarantees the desired part of the passive isolator characteristic, i.e., the payload mass characteristic, to be fully restored beyond the filter's cutoff frequency. By attending active control based on relative displacement, a small inherent performance deterioration is shown beyond resonance. Unlike the passive isolator design (see Fig. 2), the results obtained with an active design show no severe performance deterioration for small values of ϕ, i.e., for a highly nonlinear isolator characteristic. Even for the degree of nonlinearity $\phi=5$, linear vibration control seems reasonably effective in dealing with the nonlinear isolator characteristic.

4.1.2 Base Excitation. For the controlled vibration isolator model that is subjected to harmonic base excitation $x=\hat{x}\cos(2\pi ft)$ with excitation amplitude $\hat{x}$ and excitation frequency f (see Fig. 5 with $F=0$) the dimensionless equations of motion in matrix notation are given by

$$\frac{d\Xi}{d\theta}=A(\Xi,\theta)\Xi+\mathcal{K}(\Xi_4,\theta)Bu+2\zeta B\frac{du}{d\theta},\quad u=\cos(\Omega\theta) \tag{33}$$

with

$$A(\Xi,\theta)=\begin{bmatrix} 0 & 1 & 0 & 0 & 0 \\ 0 & 0 & 1 & 0 & 0 \\ 0 & -\Omega_{lp}^2 & -2\beta\Omega_{lp} & \Omega_{lp}^2 & 0 \\ 0 & 0 & 0 & 0 & 1 \\ -\alpha\dfrac{\omega_i}{\omega_n} & -\alpha\left(1+\dfrac{\omega_i}{\omega_d}\right) & -\alpha\dfrac{\omega_n}{\omega_d} & -\mathcal{K}(\Xi_4,\theta) & -2\zeta \end{bmatrix}$$

$$\text{and } B=\begin{bmatrix} 0 \\ 0 \\ 0 \\ 0 \\ 1 \end{bmatrix}$$

The vector $\Xi=[\Xi_1\ \Xi_2\ \Xi_3\ \Xi_4\ \Xi_5]^{\mathrm{T}}$—comparable to the previous case of force excitation—contains the dimensionless displacement and velocity of the payload: $\Xi_4=\xi$ and $\Xi_5=d\xi/d\theta$, respectively. Different from the previous case of force excitation, the dimensionless payload displacement ξ is given by $\xi=y/\hat{x}$, whereas $\mathcal{K}(\Xi_4,\theta)$ yields

$$\mathcal{K}(\Xi_4,\theta)=\left(\frac{\eta}{\eta+\Xi_4-\cos(\Omega\theta)}\right)^{\kappa+1} \tag{34}$$

with $\eta=L_o/\hat{x}$. Note that the degree of nonlinearity in $\mathcal{K}(\Xi_4,\theta)$ is largely determined by η, i.e., the characteristic isolator length L_o and the amplitude of base excitation $\hat{x}$. For purposes of numerical analysis, the parameter values in $A(\Xi,\theta)$ are given by $\omega_i=\omega_d=\omega_n/5$, $\omega_{lp}=5\omega_n$, $\alpha=1/10$, $\zeta=0.04$, $\kappa\approx1.402$, and $\beta=1$ (see also Sec. 4.1.1).

With Eq. (33), the results of a generalized transmissibility analysis are shown in Fig. 7. Again four curves of period-1 solutions are depicted, each computed for varying dimensionless excitation frequency Ω. The degree of nonlinearity is expressed by η. Additionally, the passive linear isolator characteristic is depicted. By comparing the passive linear isolator characteristic with the curve based on $\eta=2\times10^3$, which corresponds to an active, approximately linear, isolator characteristic, it follows that: (i) the lead filter induces additional damping near resonance, (ii) the low-pass filter guarantees the desired part of the passive isolator characteristic to be restored beyond the filter's roll-off, and (iii) an inherent performance trade-off—related to the choice for relative instead of absolute damping—is shown beyond resonance. In principle, the lag filter does not show its influence in the low-frequency range. It does, however, affect the high-frequency response. Namely, the offset value in the response of the passive nonlinear isolator model, such as studied in Sec. 3.2, is no longer present. In Fig. 7, a severe expression of nonlinearity is shown for $\eta=10$. Here the bending resonance peak implies the coexistence of unstable period-1 solutions embedded in a mainly nonperiodic large-amplitude response. Apart from this severe case of nonlinearity, the linear control design seems capable of avoiding large expressions of nonlinearity. A feature that merely results from considering harmonic excitations only. For nonharmonic excitations, this conclusion is less apparent. This is shown in Sec. 4.2 where additive nonlinear control is proposed as a means to overcome isolation performance deterioration caused by the nonsymmetric isolator characteristic.

4.2 Nonlinear Vibration Control. To avoid any expression of nonlinearity in the active vibration isolation system whatsoever, a model-based nonlinear part is added to the linear control design. Based on the concept of feedback linearization [12], an additive control force is proposed that compensates for the nonlinear part of the passive isolator characteristic. Ideally, the nonlinear terms resulting from both the isolator and the controller cancel out;

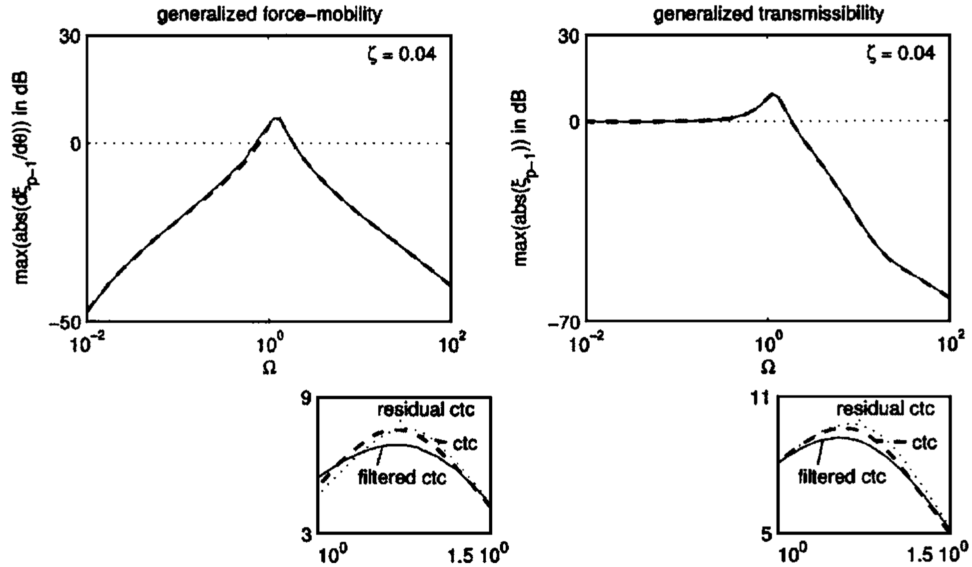

Fig. 8 Generalized force-mobility and transmissibility analysis

hence, performance can be quantified on the basis of the linear vibration isolation concept. In practice, however, a residual nonlinear term is likely to remain, for example, due to model uncertainty or actuator-sensor limitations. The effect of this term on the system response is studied: (i) by assuming parameter uncertainty in the isolator stiffness characteristic and (ii) by limiting the computed torque output using dynamic filtering.

For the case of force excitation, an additive so-called computed torque part is defined as

$$\frac{d\tilde{v}}{d\theta} = -\Omega_{lp}\tilde{v} + \Delta\Omega_{lp}v \quad \text{and} \quad v = \mathcal{K}(\Xi_4)\Xi_4 - \Xi_4 \tag{35}$$

with $\Delta = \tilde{k}/k$ accounting for uncertainty in the passive isolator stiffness coefficient, $\tilde{k}$ an estimation of the stiffness coefficient k, and Ω_{lp} the cutoff frequency of a first-order low-pass filter; $\Omega_{lp} = 5\omega_n$ with ω_n the resonance frequency resulting from a comparable but linear isolator ($\mathcal{K}(\Xi_4)=1$). The computed torque part compensates for the nonlinear spring force characteristic

$$\mathcal{K}(\Xi_4) = \left(\frac{\phi}{\Xi_4 + \phi}\right)^{\kappa+1} \tag{36}$$

with Ξ_4 the dimensionless displacement of the payload mass ($\Xi_4 = \xi$) and ϕ expressing the degree of nonlinearity in the isolator design. Apart from nonlinear force cancellation, the computed torque controller also features a linear spring force contribution. The overall nonlinear control force transforms Eq. (30) into

$$\frac{d\Xi}{d\theta} = A(\Xi)\Xi + Bu + B\tilde{v}, \quad u = \cos(\Omega\theta) \tag{37}$$

with Ω the dimensionless excitation frequency.

For the case of base excitation, the computed torque part is given by

$$\frac{d\tilde{v}}{d\theta} = -\Omega_{lp}\tilde{v} + \Delta\Omega_{lp}v \text{ and } v = \mathcal{K}(\Xi_4,\theta)\Xi_4 - \mathcal{K}(\Xi_4,\theta)u - \Xi_4 + u \tag{38}$$

Similar to the previous case of force excitation, Δ represents a measure for the amount of parameter uncertainty in the passive isolator stiffness characteristic whereas Ω_{lp} represents the cutoff frequency of a first-order low-pass filter. The nonlinear spring force characteristic $\mathcal{K}(\Xi_4,\theta)$ for which the computed torque controller is designed to account for is given by

$$\mathcal{K}(\Xi_4,\theta) = \left(\frac{\eta}{\eta + \Xi_4 - \cos(\Omega\theta)}\right)^{\kappa+1} \tag{39}$$

with Ξ_4 the dimensionless displacement of the payload mass ($\Xi_4 = \xi$), θ the dimensionless time, Ω the dimensionless excitation frequency, and η expressing the degree of nonlinearity in the passive vibration isolator. The proposed nonlinear controller consists of a part that claims nonlinear spring force cancellation and a part that, in return, induces a linear relation between input displacement and output force. The overall nonlinear controller transforms Eq. (33) into

$$\frac{d\Xi}{d\theta} = A(\Xi,\theta)\Xi + \mathcal{K}(\Xi_4,\theta)Bu + 2\zeta B\frac{du}{d\theta} + B\tilde{v}, \quad u = \cos(\Omega\theta) \tag{40}$$

With (37) and (40), the controlled vibration isolator model subjected to harmonic excitation is studied in Fig. 8 via a generalized force-mobility analysis (the left part) and a generalized transmissibility analysis (the right part).

Note that the effect of additional computed torque control follows from comparing Fig. 8 with Figs. 6 and 7, respectively. In Fig. 8, three situations are considered: (i) noncorrupted computed torque control, i.e., Eqs. (37) and (40), respectively, with $\tilde{v} := v$ (dashed lines), (ii) low-pass filtered computed torque control, i.e., Eqs. (37) and (40), respectively, with $\Delta = 1$ (solid lines), and (iii) computed torque control with uncertainty in the isolator stiffness characteristic, i.e., Eqs. (37) and (40), respectively, with $\tilde{v} := \Delta \times v$ and $\Delta = 1.1$ (dotted lines). The characteristics corresponding to noncorrupted computed torque control perfectly match with the amplitude characteristics of the linear force mobility and transmissibility function. The considered filtered computed torque signal—as a means to account for actuator limitations—does not seem to influence this result much. In more detail, this is shown in the exploded views at the bottom of Fig. 8 at $\phi = 5$ for the case of force excitation and at $\eta = 10$ for the case of base excitation. At these parameter settings, the previously considered linear control design demonstrated a severe expression of nonlinearity, recall the results shown in Figs. 6 and 7, respectively. Also an uncertainty (labeled in Fig. 8 with residual ctc) in the isolator stiffness coefficient of 10% ($\Delta = 1.1$) does not imply a significant deterioration of the controlled isolator performance. Therefore, it is concluded that nonlinear control seems able to avoid large expressions of nonlinearity in the system response. These expressions, however,

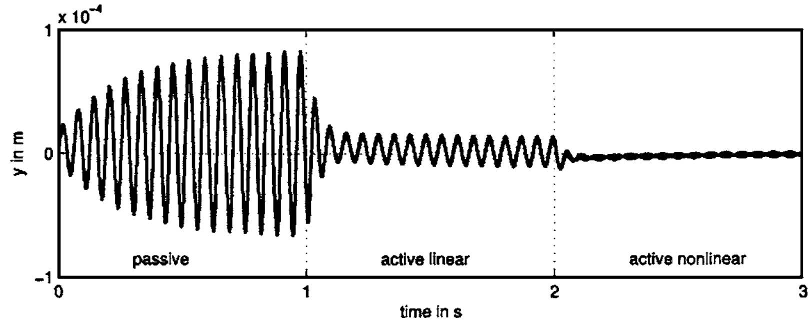

Fig. 9 Time-series computation with dual-frequency base excitation

only appeared at small values for ϕ and η. For large values of ϕ and η, nonlinear control shows little additional improvement, at least, for the considered case of harmonic excitation.

For nonharmonic excitation (such as multiple frequency excitations, possibly stochastic), the nonsymmetric nature of the vibration isolator characteristic can cause severe changes in performance, which may no longer be handled merely by the considered linear control design. This is illustrated in Fig. 9 by a time-series computation of the motion y of the isolator payload mass. Herein the case of dual base excitation is considered (see also the last part of Sec. 3.2) i.e., the system is subjected to base motion defined by

$$x=\hat{x}_1 \cos(2\pi f_1 t)+\hat{x}_2 \cos(2\pi f_2 t) \tag{41}$$

with $\hat{x}_1=\hat{x}_2=\sqrt{1/2}10^{-4}$ m, $f_i=200$ Hz, and $f_2=214.75$ Hz. Figure 9 can be divided into three parts. In the first part from 0 to 1 s, the system response is shown for the case of passive nonlinear isolation, i.e., Eq. (16) combined with Eq. (41), where $t(0)=0, y(0)=0$, and $\dot{y}(0)=0$. For $\eta=L_o/\hat{x}_1=20$ with L_o the characteristic isolator chamber length, it can be seen that dual excitation with merely high-frequency content induces a large-amplitude low-frequency response. In the second part from 1 to 2 s, the system response is shown under linear control, Eq. (33) combined with Eq. (41). Although decreased in amplitude, the response still features the characteristic large-amplitude low-frequency behavior. This illustrates the limitations of a single harmonic excitation analysis because an indication for the occurrence of such behavior could not be deduced from Fig. 7. In the last part from 2 to 3 s, the response is depicted under overall nonlinear control. Here the characteristic small-amplitude high-frequency behavior is shown, which is typical of a linear isolator model subjected to a multiple high-frequency excitation. The reduction in vibration amplitude during the transition from uncontrolled to linear controlled by a factor of $\sim$6.5 is comparable to the reduction obtained during the transition from linear controlled to nonlinear controlled by a factor of $\sim$6.2; hence, the need for nonlinear control is far more apparent from the case of multiple frequency excitation than from the earlier case of harmonic excitation.

The influence of corrupted computed torque control under multiple excitation is depicted in Fig. 10, which shows both the influence of the previously considered filtered computed torque force (the upper part) and the computed torque force based on uncertainty in the isolator stiffness coefficient of 10% (the lower part). By comparison to the case of uncorrupted computed torque control, it can be seen that the considered degree of corruption, though significant in either case, has only a limited influence on the overall characteristic system performance. Therefore, it is concluded that computed torque control, possibly corrupted, can significantly improve the vibration isolation properties. Note that

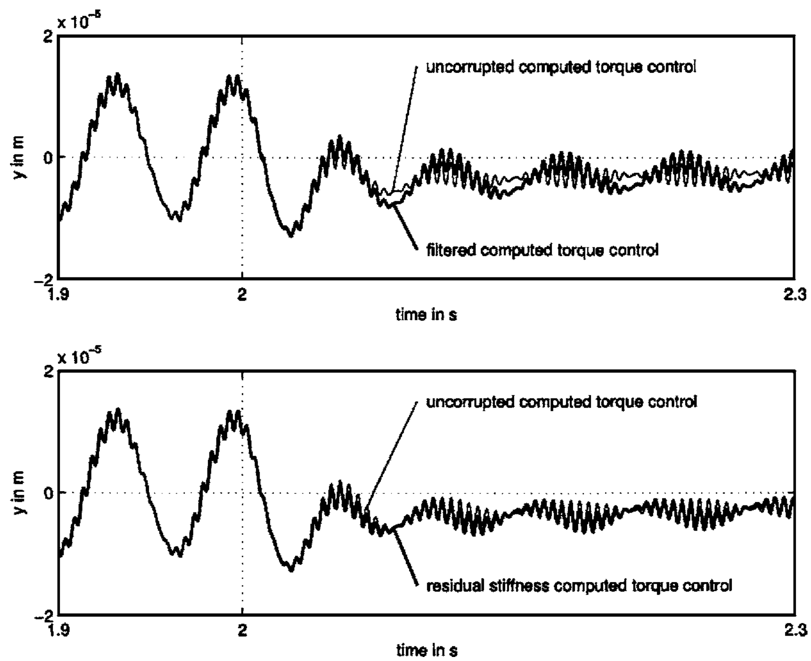

Fig. 10 Time-series computation with computed torque control: low-pass filtered (upper part) and with parameter uncertainty of $\Delta=1.1$ (lower part)

when the computed torque controller is corrupted (thick lines), a nonsymmetric response remains due to residual nonlinearity in the system.

5 Conclusions

To study the behavior of nonlinear pneumatic vibration isolators within the vibration isolation context, a single-degree-of-freedom nonlinear model based on a physical nonsymmetric stiffness nonlinearity is derived.

With this model, the sensitivity of a payload mass to harmonic-force excitation is studied on the basis of the generalized force-mobility function. Depending on the system properties, the nonsymmetric nonlinearity is shown to seriously compromise the low-frequency vibration isolation characteristics either by bending of the resonance peak yielding the coexistence of steady-state solutions, or by the occurrence of a superharmonic resonance.

The sensitivity of the payload mass to harmonic base excitation is studied on the basis of the generalized transmissibility function. Again, the effect of the nonsymmetric nonlinearity on the isolation performance is shown via a bending resonance peak, but also by the occurrence of a subharmonic response. Moreover, the nonsymmetric nonlinearity is shown to have the potential of inducing high-energy low-frequency response to high-frequency excitation consisting of multiple frequencies. To avoid such behavior, or, more importantly, its deteriorating impact on the vibration isolator performance, a nonlinear feedback control design is proposed. This design consists of two parts: a linear PID-based controller and a model-based nonlinear computed torque controller. The PID-based controller is used to shape the passive linear isolator characteristics. The computed torque controller is used to achieve nonlinear force cancellation giving overall linear isolator dynamics.

Both for the case of harmonic-force and base excitation, it is shown that active vibration isolation based on linear control seems reasonably effective in dealing with isolator nonlinearity. For the case of multiple-frequency base excitation, however, it is shown that active vibration isolation primarily based on linear control still enables a significant expression of nonlinearity in the system response.

The combined linear and nonlinear control design results in the desired low-amplitude (possibly high-frequency) response, thus attaining a higher isolator performance. A brief robustness study of this control design against model uncertainty and sensor-actuator limitations shows that nonlinear control can significantly improve the isolator performance.

References

[1] Snowdon, J. C., 1979, "Vibration Isolation: Use and Characterization," J. Acoust. Soc. Am., **66**, pp. 1245–1279.

[2] Subrahmanyan, P. K., and Trumper, D. L., 2000, "*Synthesis of Passive Vibration Isolation Mounts for Machine Tools: A Control Systems Paradigm*," Proc. of American Control Conf., IEEE, Chicago, pp. 2886–2891.

[3] Freudenberg, J., Middleton, R., and Stefanopoulou, A., 2000, "*A Survey of Inherent Design Limitations*," Proc. of American Control Conference, IEEE, Chicago, pp. 2987–3001.

[4] Natsiavas, S., 1992, "Steady-State Oscillations and Stability of Non-linear Dynamic Vibration Absorbers," J. Sound Vib., **156**(2), pp. 227–245.

[5] Chandra Shekhar, N., Hatwal, H., and Mallik, A. K., 1998, "Response of Nonlinear Dissipative Shock Isolators," J. Sound Vib., **214**(4), pp. 589–603.

[6] Ravindra, B., and Mallik, A. K., 1994, "Performance of Non-Linear Vibration Isolators Under Harmonic Excitation," J. Sound Vib., **170**(3), pp. 325–337.

[7] Erin, C., and Wilson, B., 1998, "An Improved Model of a Pneumatic Vibration Isolator: Theory and Experiment," J. Sound Vib., **218**(1), pp. 81–101.

[8] Beard, A. M., Schubert, D. W., and Flotow, von A. H., 1994, "A Practical Product Implementation of an Active/Passive Vibration Isolations System," Proc. SPIE, **2264**, pp. 38–49.

[9] Hyde, T. T., and Crawley, E. F., 1995, "$\mathcal{H}_2$ Synthesis for Active Vibration Isolation," *Proc. of American Control Conference*, IEEE, Seattle, pp. 3835–3839.

[10] Nagaya, K., and Kanai, H., 1995, "Direct Disturbance Cancellation With an Optimal Regulator for a Vibration Isolation System with Friction," J. Sound Vib., **180**(4), pp. 645–655.

[11] Royston, T. J., and Singh, R., 1996, "Optimization of Passive and Active Non-linear Vibration Mounting Systems Based on Vibratory Power Transmission," J. Sound Vib., **194**(3), pp. 295–316.

[12] Isidori, A., 1995, *Nonlinear Control Systems*, Third Edition, Springer, New York.

[13] Oliva, A. I., Aguilar, M., and Sosa, V., 1998, "Low- and High-Frequency Vibration Isolation for Scanning Probe Microscopy," Meas. Sci. Technol., **9**, pp. 383–390.

[14] Heertjes, M. F., Sperling, F. B., and Van de Molengraft, M. J. G., 2001, "Computing Periodic Solutions for a CD-Player with Impact using Piecewise Linear Shooting," *Proc. of Conf. on Decision and Control*, IEEE, Orlando, pp. 2195–2200.

[15] Amick, H., 1997, "On Generic Vibration Criteria for Advanced Technology Facilities," J. Inst. Env. Sci., **5**, pp. 35–44.

[16] Zi-QiangLang, and Billings, S. A., 1997, "Output Frequencies of Nonlinear Systems," Int. J. Control, **67**(5), pp. 713–730.

[17] Van de Wouw, N., Nijmeijer, H., and Van Campen, D. H., 2002, "Approximation of Stochastic Nonlinear Dynamics: A Volterra Series Approach," Nonlinear Dyn., **27**, pp. 397–409.